THE JOURNAL OF PHYSICAL CHEMISTRY A

ARTICLE

pubs.acs.org/JPCA

Theoretical Calculations of Hyperfine Coupling Constants for Muoniated Butyl Radicals

Ya Kun Chen, Donald G. Fleming, and Yan Alexander Wang*

Department of Chemistry, University of British Columbia, 2036 Main Mall, Vancouver, British Columbia V6T 1Z1, Canada

Supporting Information

ABSTRACT: The hyperfine coupling constants (HFCCs) of all the butyl radicals that can be produced by muonium (Mu) addition to butene isomers (1- and 2-butene and isobutene) have been calculated, to compare with the experimental results for the muon and proton HFFCs for these radicals reported in paper II (Fleming, D. G.; et al. J. Phys. Chem. A 2011, 10.1021/jp109676b) that follows. The equilibrium geometries and HFCCs of these muoniated butyl radicals as well as their unsubstituted isotopomers were treated at both the spin-unrestricted MP2/EPR-III and B3LYP/EPR-III levels of theory. Comparisons with calculations carried out for the EPR-II basis set have also been made. All calculations were carried out in vacuo at 0 K only. A C−Mu bond elongation scheme that lengthens the equilibrium C−H bond by a factor of 1.076, on the basis of recent quantum calculations of the muon HFCCs of the ethyl radical, has been exploited to determine the vibrationally corrected muon HFCCs. The sensitivity of the results to small variations around this scale factor was also investigated. The computational methodology employed was "benchmarked" in comparisons with the ethyl radical, both with higher level calculations and with experiment. For the β-HFCCs of interest, compared to B3LYP, the MP2 calculations agree better with higher level theories and with experiment in the case of the eclipsed C−Mu bond and are generally deemed to be more reliable in predicting the equilibrium conformations and muon HFCCs near 0 K, in the *absence* of environmental effects. In some cases though, the experimental results in paper II demonstrate that environmental effects enhance the muon HFCC in the solid phase, where much better agreement with the experimental muon HFCCs near 0 K is found from B3LYP than from MP2. This seemingly better level of agreement is probably fortuitous, due to error cancellations in the DFT calculations, which appear to mimic these environmental effects. For the staggered proton HFCCs of the butyl radicals exhibiting no environmental effect in paper II, the best agreement with experiment is consistently found from the B3LYP calculations, in agreement also with benchmark calculations carried out for the ethyl radical.

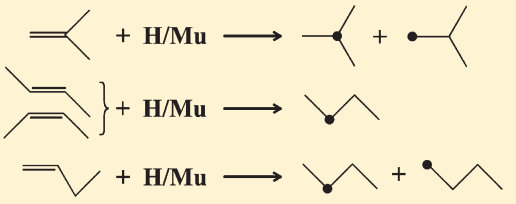

INTRODUCTION AND BACKGROUND

Free radicals are reactive chemical species with unpaired electrons that are of long-standing interest, having largely fostered the development of electron paramagnetic resonance (EPR) spectroscopy over decades as a powerful tool for the study and characterization of these spin-polarized systems. An important aspect in this development has been the study of D-atom isotopic effects. However, since H and D atoms differ by only a factor of 2 in mass, their EPR isotopic effects are relatively minor. With the development of nuclear science techniques, the muonium atom (Mu = μ^+e^-) with a positive muon (μ^+) for the nucleus, a radioactive and almost 100% spin-polarized elementary particle, has emerged as a remarkably light H-atom isotope (m_{Mu} = 0.113 amu). The muon spin resonance (μSR) technique,[1,2] an EPR analogue for characterizing Mu-containing species, has been widely employed to study isotopic effects in a number of chemical systems, including both Mu formation and reaction rates,[3−5] and of particular interest here, muoniated free radicals.[1]

A central measurement in free radical studies, either by EPR or by μSR, is the isotropic hyperfine coupling constant (HFCC) that arises from the interaction between unpaired electrons and nuclear spins, and which provides valuable electronic structural information about the free radical under study. In the past decade alone, the HFCCs of various muoniated radicals have been obtained and often characterized with the aid of theory in a wide variety of host media and molecular environments.[6−13] The present paper focuses on calculations of HFCCs for muoniated butyl radicals at 0 K, in part to help explain the experimental data discussed in the paper that follows, hereafter referred to as paper II.[14] To our knowledge, there have been no previous detailed and systematic ab initio calculations of the HFCCs of butyl radicals beyond the early INDO results of Krusic et al.[15] and the later UHF study of Carmichael for the *tert*-butyl radical[16,17] and of Overill,[18] also for *tert*-butyl, only. The only reference to previous calculations of muon HFCCs in butyl radicals appears to also be from the early work of Carmichael for the muoniated *tert*-butyl radical,[17] though mainly focused on the trend for the temperature dependence of these HFCCs.

The HFCC is proportional to the electron spin density at the nucleus of interest. At first glance, it might seem that any theoretical method that can be used to calculate the electron spin density should be amenable to the calculation of HFCCs.

Received: October 7, 2010
Revised: February 4, 2011
Published: March 11, 2011

However, these methods can often fail dramatically in calculating HFCCs because most are designed to give a good description of valence-shell electron interactions so that other molecular properties, such as bond lengths and atomization energies, can be satisfactorily predicted.

An early attempt to predict HFCCs by ab initio methods can be found in Meyer's 1969 Hartree−Fock (HF) calculations.[19] However, due to its lack of electron correlation, the HF method was found unsuitable to yield quantitative results for HFCCs. Even though several post-HF methods that were subsequently developed, such as configuration interaction theory (CI),[20] the multiconfiguration self-consistent-field (MCSCF) method[21] and coupled cluster (CC) theory,[22,23] were able to include electron correlation effects, these post-HF methods are usually too demanding on computational resources for routine use in HFCC calculations, even for medium size molecules. Typically, second-order Møller−Plesset perturbation theory (MP2) can recover more than 80% of electron dynamic correlation effects and has been successful at reproducing experimental HFCCs at acceptable computational cost.[24,25] Accordingly, we have employed MP2 here.

An alternative method to obtain HFCCs is to use density functional theory (DFT), which has become popular in the past decade for its speed and accuracy. This is particularly true for proton HFCC calculations, confirmed by a recent regression analysis that indeed showed DFT to be a promising tool.[26] Nevertheless, the use of approximate exchange−correlation functionals limits the broad utility of the DFT method in the calculation of HFCCs, because the good agreement often found between DFT calculations and experimental results can stem from error cancellations.[27] Several examples of this artifact can be found, for example, in the calculations of HFCCs for some metal complexes, regardless of the form of the density functionals employed.[28] This appears to be the case as well for some specific muoniated butyl radicals, depending on environment, as discussed below.

Besides the form of the Hamiltonian adopted in theoretical investigations, the quality of the basis set in a HFCC calculation also plays an important role.[18,20,29,30] To obtain accurate electron (and spin) density near a nucleus of interest,[31,32] basis sets, such as EPR-II and EPR-III, which were specially tailored for EPR studies, are always much preferred.[33]

Moreover, it is essential to have good geometric parameters to calculate HFCCs, because the electron density at each nucleus is very sensitive to molecular structural changes.[31,32] Although some theoretical studies have shown that HFCCs of small rigid molecules are often not very sensitive to different computational methods and basis sets employed,[26] that is not the case in the present study. The muoniated adducts formed from muonium addition to butene isomers are complicated geometrically due to the flexible aliphatic chains of the resultant radical isomers, especially those formed from 1-butene. In such cases, theoretical methods must be carefully selected to meet geometric requirements.

Early studies showed that MP2 could be unsatisfactory in calculating the formation processes of alkyl radicals by atom addition to alkenes because of large spin contamination, which indicates that MP2 calculations could have a potentially negative impact on the reliability of calculations of HFCCs of these radical systems.[34,35] On the other hand, DFT methods have also proven inadequate for some conformational calculations due to their inability to account for weak, noncovalent, interactions.[36−40] Since both DFT and MP2 methods have their merits and shortcomings in determining the stationary conformations of open-shell species from different perspectives, we have thoroughly benchmarked their performance against other high-level theories and various density functionals with different basis sets (see the Supporting Information). In the end, both DFT and MP2 methods utilizing the EPR-III basis set have been employed and compared in this study of butyl radical HFCCs, on the basis of considerations of a balance between accuracy and efficiency.

Beyond concerns about the electronic structure and molecular geometry, quantitative HFCC calculations of molecular free radicals also demand the inclusion of dynamic and thermal corrections. Even at 0 K, atoms in a molecule vibrate around their equilibrium positions, so the HFCC of each atom is constantly changing from its value at a fixed equilibrium position. When the temperature increases, higher vibrational states become populated, causing even larger-amplitude vibrations compared with zero-point vibrations, and further thermal corrections need to be considered in calculating temperature-dependent HFCCs to obtain quantitative agreement with experiment. This vibrational effect is particularly important in the present study, due to the very light mass of Mu, only one-ninth that of the H atom. A scheme to compensate for this vibrational effect is introduced below.

Since higher temperatures facilitate the population of higher vibrational states, this increases the deviation of β-Mu from its preferred "eclipsed" configuration at 0 K that corresponds to the maximum overlap between the C−Mu (or C−H) bond and the half-filled p_z orbital at the radical center. The HFCC of the eclipsed muon or proton decreases then when the temperature increases, and concurrently the corresponding proton HFCC at the "staggered" position increases. For alkyl radicals, it is the torsional barrier to the internal rotation about the $C_\alpha-C_\beta$ bond that mainly determines the temperature dependence of the β muon/proton HFCCs. Qualitatively speaking, a high torsional barrier translates into a late onset of HFCC change with increasing temperature and a shallow slope in the temperature-dependent region in the muon/proton HFCC plots. These barriers have been determined phenomenologically for the muoniated butyl radicals reported on in paper II, by fitting the measured temperature dependences of both proton and muon HFCCs to a model potential in which the calculated values predicted herein provided essential input.

As alluded to above, the actual HFCCs of a free radical can also be affected by its environment and particularly in the solid phase due to intermolecular ("host−guest") interactions with surrounding molecules, evidence for which has been reported by Percival and co-workers in an early μSR study of the *tert*-butyl radical,[41] where the muon HFCCs exhibit a dramatic increase in the solid phase at the bulk melting point. Similar results are seen in *cis*- and *trans*-2-butyl radicals discussed in paper II. Smaller changes in muon HFCCs, at the few percent level, have also been reported in μSR studies of solvent effects on the HFCCs of the Mu−cyclohexadienyl radical in the gas and liquid phases[42] and in polar environments[43] and for the $MuCH_2$ radical in ketene environments,[8] depending on dielectric constant and polarizability.

Though environmental effects such as those mentioned above can be important, even in the largely nonpolar media of butyl radicals, a first-principles computation of temperature-dependent HFCCs that combines both vibrational and environmental effects is well beyond the scope of the present paper. Thus, only in vacuo calculations of the HFCCs of butyl radicals at 0 K are reported, to provide a basis for comparison with the experimental data in paper II that follows. Some qualitative discussion of environmental effects affecting these HFCCs is also presented.

METHODOLOGY AND RESULTS

Some Remarks on the Calculations. Though it is recognized that non-Born−Oppenheimer effects may play an important role in calculating the properties of Mu-containing radicals, all calculations in this study are within the framework of the Born−Oppenheimer (BO) approximation. Explicit non-BO calculations are still prohibitive at present for the butyl radicals of interest here. Perhaps the most explicit demonstration of corrections to the BO approximation in Mu systems to date is found in a study of barrier heights for the isotopomers of the H_3 reaction system.[44] Not surprisingly, the largest correction is for the Mu + H_2 reaction rate, but even so the correction to the barrier height is only 3.8%. We can expect an even smaller correction to the C−Mu bond in the case of the muoniated butyl radicals studied here.

Both spin-unrestricted B3LYP[45,46] DFT and MP2 methods with EPR-III basis sets[33] implemented in Gaussian 03[47] have been used to obtain the equilibrium structures and the HFCCs of all butyl radical isomers. This particular choice of computational methods, a balance of accuracy and speed, as noted above, is based on a series of thorough numerical tests of the effects of different Hamiltonians and basis sets on the torsional potential energy surface of the *sec*-butyl radical (see the Supporting Information). Some comparisons of results obtained with the EPR-II basis set are also presented below.

Besides the pure electronic structure effect, the importance of incorporating vibrational corrections in HFCC calculations is well-known, as discussed in a recent review article.[32] As already mentioned, vibrational corrections are particularly important for C−Mu bonds in muoniated radicals,[8,48] and of particular relevance here are earlier studies of the muoniated ethyl radical.[49−51] Though the HFCCs of several small radicals have been calculated in Barone's group with the inclusion of vibrational corrections by a fully automated second-order perturbative approach implemented locally in Gaussian03,[52] this implementation is generally not available to other Gaussian03 users. In the current study of muoniated butyl radicals, lacking a direct analytical first-principles evaluation of the dynamical effect of vibrational averaging, the C−Mu bond has been intentionally elongated to 1.076 times the corresponding equilibrium C−H bond length and calculations have been carried out on this modified (static) geometry to account for contributions to HFCCs from averaging over vibrational anharmonicity in the C−Mu bond stretch. This factor is based on the recent quantum calculations of Böhm et al. for the muoniated ethyl radical[53] and is justified below. For convenience, all muon HFCC values reported here are in "reduced" units, $A'_\mu = A_\mu/3.184$, which corrects for the gyromagnetic ratio between muon and proton, thereby allowing their direct comparison as well as with the experimental results in paper II. The spin contamination was monitored and found insignificant for all the radical species studied.

Geometries and Molecular Structures. The first step in a calculation of the HFCCs of the butyl radicals of interest is to determine their equilibrium geometries. As noted earlier, all calculations were carried out within the BO framework using the Gaussian 03 package. This means that all nuclei in these radicals are depicted to move on a potential energy surface. As a consequence, the electronic Hamiltonian is independent of the nuclear mass and all isotopomers have the same equilibrium geometries and electronic structures, so the optimized conformations of muoniated butyl radicals can be discussed in terms of the corresponding hydrogen isotopomers without loss of generality. The reaction schemes for Mu (or H atom) addition to butene isomers and the corresponding optimized radical adducts formed are shown in Figures 1 and 2, with the optimized structures for 1-butene shown separately in Figure 3. The geometric optimization results are discussed individually in the following paragraphs. Conventional or common names of these species are typically used, though IUPAC names are also sometimes cited.

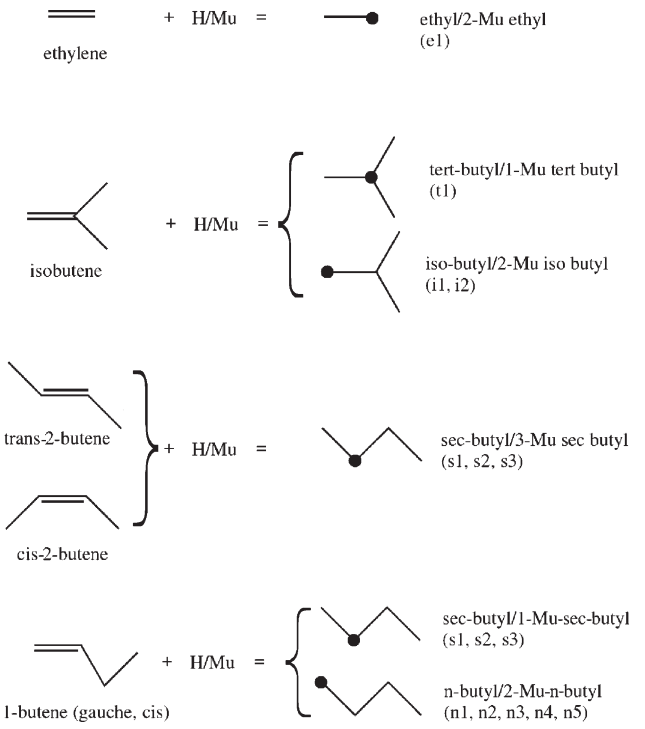

Figure 1. Hydrogen or muonium atom addition to different butene isomers. Only the carbon skeleton is shown. The dots on the product side indicate locations of the radical center. The identification of possible conformers are given in parentheses with their corresponding geometries displayed in Figures 2 and 3.

The isobutene precursor has only one geometric isomer with four coplanar carbon atoms. Hydrogen addition to the carbon double bond of isobutene results in two isomers: a *tert*-butyl and an isobutyl radical (Figure 1). The B3LYP calculations identified only one conformational isomer for each of these two radical products (t and i1 in Figure 2). However, two conformational isomers were found for isobutyl at the MP2 level. In addition to i1 (Figure 2b), a conformational isomer i2 (Figure 2c) was also found with its singly occupied p_z orbital on the radical center aligning with one of the β methyl groups, instead of aligning with a hydrogen atom as in the i1 structure. However, this i2 structure does not correspond to the direct product of Mu/H addition to isobutene and moreover the isobutyl radical is not discussed in paper II and so is not discussed further here either. Several earlier calculations of the equilibrium structure, giving C_{3v} "pyramidal" symmetry, and HFCCs of the *tert*-butyl radical at the UHF level, have been reported.[16−18] The equilibrium structure for *tert*-butyl found in the present study (Figure 2a) is close to C_{3v} but not identical to it.

For the 2-butene precursors, textbook knowledge tells us that there are both cis (less stable) and trans (more stable) isomers, and both isomers were confirmed by the MP2 and B3LYP calculations carried out here. Supported by the large and distinct

dx.doi.org/10.1021/jp1096212 |J. Phys. Chem. A 2011, 115, 2765–2777

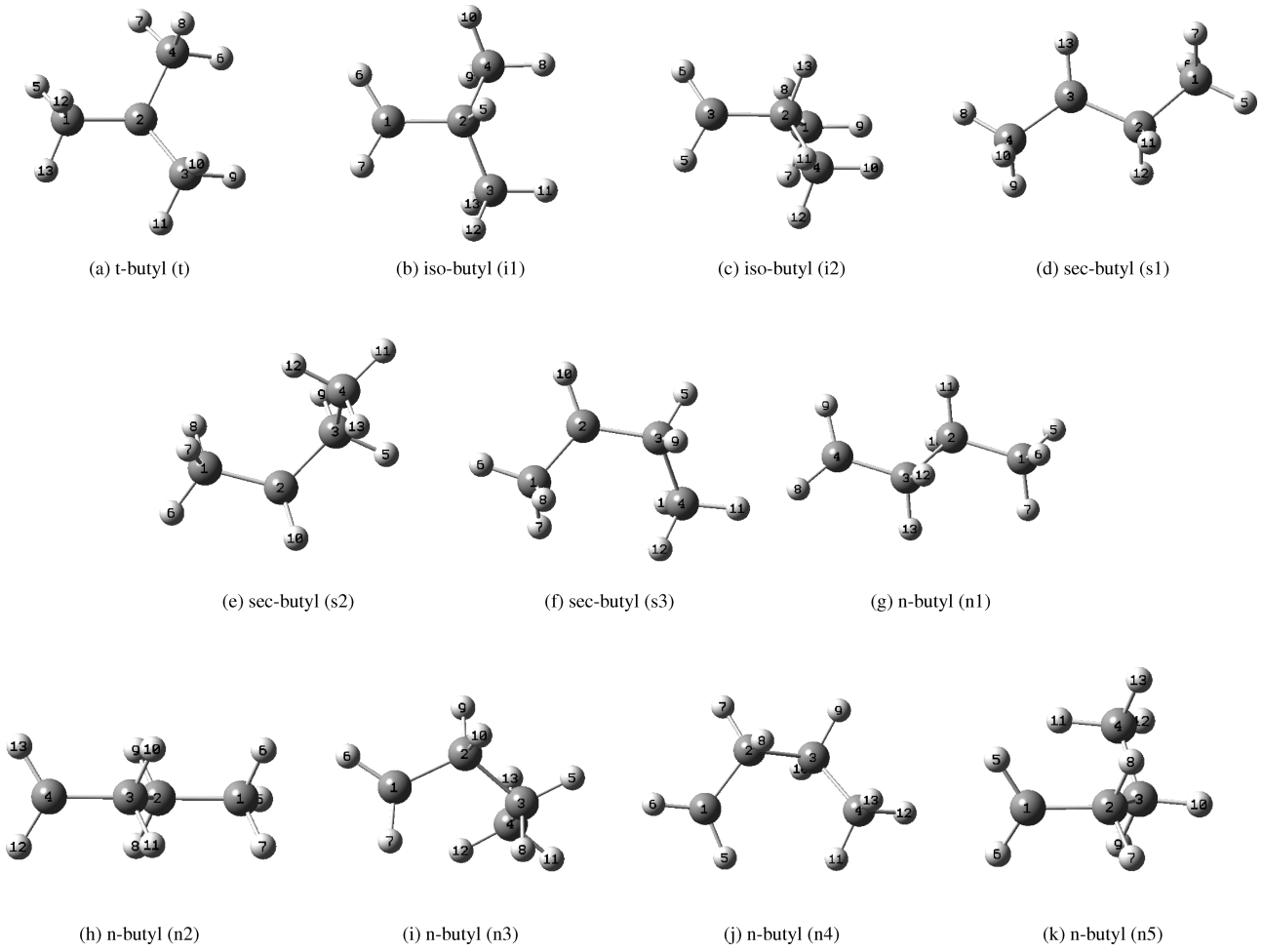

(a) t-butyl (t) (b) iso-butyl (i1) (c) iso-butyl (i2) (d) sec-butyl (s1)

(e) sec-butyl (s2) (f) sec-butyl (s3) (g) n-butyl (n1)

(h) n-butyl (n2) (i) n-butyl (n3) (j) n-butyl (n4) (k) n-butyl (n5)

Figure 2. Optimized structures of ethyl, *tert*-butyl, isobutyl, *sec*-butyl, and *n*-butyl radicals. H and C atoms are shown by small (light) and large (dark) numbered spheres, respectively.

muon HFCC values reported in paper II, one would expect the *sec*-butyl radicals formed by H/Mu addition to *trans*- or *cis*-2-butene to be s1 (Figure 2d) and s3 (Figure 2f), respectively. The B3LYP calculations identified only two structures: the expected trans conformation s1 (Figure 2d), corresponding to the product of hydrogen addition to *trans*-2-butene, but also a gauche conformation s2 (Figure 2e), which is not directly associated with either of the 2-butene precursors. On the other hand, the MP2 calculations, in addition to these two isomers from B3LYP, also found the cis structure s3 (Figure 2f), corresponding to the radical formed from hydrogen addition to *cis*-2-butene. Since the s2 (gauche) structure has a dihedral angle of the carbon backbone of about 90° and has no eclipsed β hydrogens, it is not expected to be observed near 0 K in the muon experiments reported in paper II. Though there could be some contribution from this s2 conformer at high temperatures, this structure will also not be discussed further here.

The most problematic cases in the present study are the 1-butene conformers and their muonium adducts. To the best of our knowledge, the relative stability of the gauche and cis conformations of 1-butene (Figure 3) is still ambiguous, despite the fact that their existence is well acknowledged both theoretically and experimentally. On the basis of far-infrared spectra (FIR) of 1-butene, Bell and co-workers suggested the *cis*-1-butene isomer to be 0.8 kJ/mol more stable than the gauche one.[54] In the same study, up to fourth-order Møller−Plesset perturbation theory (MP4) was employed to

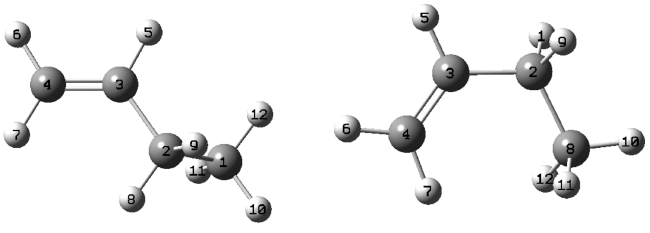

(a) gauche (b) cis

Figure 3. Optimized gauche and cis conformations of 1-butene. H and C atoms are shown by small (light) and large (dark) numbered spheres, respectively.

calculate the electronic energies of the two isomers, but the computational results contradicted the order of relative stability derived from the FIR data. The experimental results, though, were supported by an earlier study of microwave spectra.[55]

We have also carried out CCSD/cc-pVDZ calculations in addition to MP2 and B3LYP calculations on both 1-butene isomers. The gauche conformation was predicted to be the global minimum by all three theoretical methods applied. Though some experimentalists have believed that the cis conformation of 1-butene is more stable than the gauche form at low temperatures, it is worth noting that the gauche form has always been determined to be relatively more abundant than the cis form in all

Table 1. Calculated Proton and Muon HFCCs of Butyl and Mu−Butyl Isomers[a]

Radical	atom 5	atom 6	atom 7	atom 8	atom 9	atom 10	atom 11	atom 12	atom 13	theoretical method
tert-butyl	22.90	22.78	22.87	117.35	22.77	117.37	22.90	117.32	22.75	MP2/EPR-III (H)
	30.63	29.70	30.59	133.06	29.76	133.26	30.61	133.13	29.63	B3LYP/EPR-III (H)
	21.47	22.03	22.89	115.94	22.01	115.97	22.91	*131.14*	21.32	MP2/EPR-III (Mu)
	28.48	27.98	29.72	130.51	28.04	130.70	29.75	*153.72*	27.51	B3LYP/EPR-III (Mu)
isobutyl	117.91	−64.53	−64.53	0.40	−2.50	−1.30	0.40	−1.30	−2.50	MP2/EPR-III (H)
	140.05	−61.26	−61.26	0.44	−1.92	−1.50	0.44	−1.50	−1.92	B3LYP/EPR-III (H)
	129.89	−63.87	−63.87	0.39	−1.22	−2.70	0.39	−1.22	−2.70	MP2/EPR-III (Mu)
	159.81	−57.77	−57.77	0.53	−2.17	−1.36	0.53	−1.36	−2.17	B3LYP/EPR-III (Mu)
sec-butyl (si)	−1.88	−2.21	−1.49	12.29	46.42	125.69	113.85	47.16	−60.03	MP2/EPR-III (H)
	−2.10	−1.76	−1.57	12.85	66.24	137.36	126.70	66.65	−61.44	B3LYP/EPR-III (H)
	−1.83	−2.49	−1.44	11.76	46.48	124.14	*127.36*	45.44	−59.02	MP2/EPR-III (Mu + 2-butene)
	−1.89	−2.06	−1.44	11.47	65.31	134.62	*145.17*	64.10	−57.74	B3LYP/EPR-III (Mu + 2-butene)
	−1.88	−2.19	−1.46	11.34	44.71	*139.55*	113.44	47.20	−58.98	MP2/EPR-III (Mu + 1-butene)
	−1.88	−1.55	−1.36	11.39	63.51	*157.28*	124.17	65.75	−57.69	B3LYP/EPR-III (Mu + 1-butene)
sec-butyl (s2)	14.40	22.92	131.61	34.08	34.22	−60.93	11.63	−3.84	−3.40	MP2/EPR-III (H)
	34.38	20.51	148.24	55.90	28.12	−60.86	12.11	−4.14	−3.42	B3LYP/EPR-III (H)
	14.11	21.70	*145.95*	32.64	34.36	−59.94	11.07	−3.84	−3.41	MP2/EPR-III (Mu + 1-butene)
	32.52	18.13	*168.32*	52.78	26.92	−54.12	11.91	−3.72	−3.03	B3LYP/EPR-III (Mu + 1-butene)
sec-butyl (s3)	8.15	−0.53	77.52	109.71	110.81	−62.64	0.10	−2.01	−2.52	MP2/EPR-III (H)
	7.33	−0.65	77.15	108.13	*123.98*	−61.69	0.17	−1.95	−2.81	MP2/EPR-III (Mu + *cis*-2-butene)
	7.79	−0.88	75.30	*121.75*	110.27	−61.66	0.21	−1.99	−2.52	MP2/EPR-III (Mu + 1-butene)
1-butyl (n1)	−0.65	0.44	0.48	−66.07	−65.52	−2.54	−1.54	130.21	36.84	MP2/EPR-III (H)
	−0.18	0.82	0.85	−62.03	−62.13	−2.14	−1.73	150.28	54.32	B3LYP/EPR-III (H)
	−0.79	0.59	0.44	−65.41	−64.82	−2.80	−1.49	*143.46*	35.52	MP2/EPR-III (Mu + 1-butene)
	−0.30	1.05	0.76	−55.92	−55.97	−2.22	−1.44	*169.84*	51.67	B3LYP/EPR-III (Mu + 1-butene)
1-butyl (n3)	−2.57	−66.26	−64.96	−1.55	35.32	134.81	−1.56	2.07	0.08	MP2/EPR-III (H)
	−2.62	−62.30	−61.34	−1.86	41.61	157.73	−0.82	2.42	0.50	B3LYP/EPR-III (H)
	−2.53	−65.58	−64.23	−1.44	34.05	*148.62*	−1.58	2.19	0.01	MP2/EPR-III (Mu + 1-butene)
	−2.44	−58.72	−57.70	−1.63	39.70	*179.42*	−0.89	2.62	0.44	B3LYP/EPR-III (Mu + 1-butene)
1-butyl (n4)	−63.75	−65.04	36.01	122.38	1.00	−2.16	0.94	0.43	−0.20	MP2/EPR-III (H)
	−63.02	−64.36	34.70	*134.94*	1.05	−2.40	0.91	0.28	−0.23	MP2/EPR-III (Mu + 1-butene)

[a] Atoms are labeled according to Figure 2. In the last column, the "H" in parentheses denotes that the HFCCs were calculated at their equilibrium structures for the unsubstituted radicals (H atoms only). The "Mu" in parentheses means that the HFCC highlighted in italic was calculated on the basis of the structure where the C—Mu bond was intentionally stretched to 1.076 times the equilibrium C−H bond length. The HFCC values for 1-butyl (n4) were based on the geometry from MP2/EPR-II calculations.

three commonly accessible phases (gas, liquid, and solid).[56] This is also the case in a recent electron momentum spectroscopy investigation of 1-butene in the gas phase, where the gauche (or "skew") conformer was favored over the cis (or "syn") form by a mole ratio of 2:1.[57] These experimental results, combined with our theoretical predictions, lead us to believe that the gauche form is indeed the more stable form and is thus the main 1-butene precursor in the experiments reported in paper II. Therefore, our theoretical effort here is focused on the corresponding Mu or H atom adducts to this gauche form.

Though the isotopic labeling is different and hence the μSR results in paper II are distinctly different for Mu addition to 1-butene or 2-butene, H/Mu addition to the terminal unsaturated carbon atom of 1-butene results in the same equilibrium structure for the *sec*-butyl radical formed as in addition to 2-butene. On the basis of stereochemistry and our calculations, the s1 and s2 conformations are the *sec*-butyl radicals formed from H addition to the terminal carbon of gauche 1-butene from the less and the more hindered side, respectively. The s3 structure (Figure 2f) is associated with addition to the terminal double bond carbon atom of *cis*-1-butene and is expected to be less important experimentally.

Hydrogen/muonium can also add to the nonterminal double bond carbon atoms in 1-butene, forming the *n*-butyl (or 1-butyl) radicals (n1 to n5 in Figure 2g−k). The B3LYP calculations for *n*-butyl located three local minima (n1, n2, and n3), whereas the MP2 calculations located all five of them (n1−n5). The n3 and n1 butyl conformations can be designated as the radicals produced from H addition to the nonterminal carbon atom of the double bond of gauche-1-butene from the less hindered and more hindered side, where the presence of the ethyl group hinders the attack of H/Mu, respectively. The n3 radical is then the more stable form. The n4 butyl radical stems from hydrogen addition to *cis*-1-butene. The other two isomers, n2 and n5, are not directly associated with any reaction products formed by hydrogen addition to 1-butene isomers at low temperatures, so these two structures are also not discussed further in this study. Again though they might contribute to experiments at higher temperatures.

Overview and Calculated HFCCs. On the basis of the optimized geometries discussed above, the HFCCs calculated at the B3LYP/EPR-III and MP2/EPR-III levels of theory are listed in Table 1. The HFCC on any nucleus of a free radical is proportional to the electron spin density on that nucleus and can be decomposed into two contributions: the direct (delocalization) contribution from the singly occupied molecular orbital and the indirect spin polarization contribution due to electron correlation effects.[32,58] In this study, the spin density on the eclipsed β-hydrogen was found to be much larger than that on the staggered hydrogen(s) because the eclipsed β-hydrogen atom can share some spin density with the aligned half filled p_z orbital via hyperconjugation, consistent with what is known for muoniated alkyl radicals.[13,17,41,50] Therefore, the large muon HFCCs seen near 0 K for the muoniated *sec*-butyl radicals in paper II can be assigned to eclipsed conformations. This is also true for some proton HFCCs reported in paper II. Another fact in support of assigning eclipsed structures at 0 K to these radicals is

Table 2. Experimental and Theoretical HFCCs (in MHz) for Protons in Unsubstituted Ethyl and for Muons and Protons in Muoniated Ethyl, Mainly at 0 K[a]

Isotopomer	β H (eclipsed)	β H (staggered)	$\langle A_\beta \rangle$, β H (averaged)	α H	theoretical method
ethyl	141.4	31.8	68.4	−67.2	MP2/EPR-III
	162.7	40.2	81.1	−62.9	B3LYP/EPR-III
	137.0	31.6	66.7	−67.3	MP4/EPR-III
	139.8	33.8	69.1	−71.1	CCSD/EPR-III
	135.1	31.9	66.3	−72.7	QCISD(T)/DZP[20]
			69.3	−65.7	QCISD(T)/TZP[20]
			68.7	−62.6	vibrationally corrected QCISD(T)/TZP[20]
			65.0	−68.0	CCSD(T)/TZ2P[22]
			65.2	−72.3	CCSD(T)/Chipman basis set[22]
			76(1)	−63(1)	ethyl experimental[13,63] (errors in parentheses)
Mu−ethyl	156.1	30.6	72.5	−66.5	MP2/EPR-III (elongated C−Mu bond)
	184.7	37.9	86.8	−58.3	B3YLP/EPR-III (elongated C−Mu bond)
	195.0	42.6	93.4	−46.8	B3LYP/EPR-III//tight-binding equilibrium structure[53]
	151(2)	36(2)	80(2)	−60(1)	Mu−ethyl experimental[13,63] (errors in parentheses)

[a] The MP2/EPR-III and B3LYP/EPR-III calculations for the Mu−ethyl radical were carried out on a modified geometry whose C—Mu bond was stretched to 1.076 times the equilibrium C−H bond length.

that the incoming Mu/H attacks preferentially to the C═C double bond from the p_π orbital direction and this naturally leads to eclipsed radical products.[59]

The proton HFCCs are usually satisfactorily obtained at the B3LYP level of theory in the present study, particularly for the staggered protons of muoniated alkyl groups, which are typically underestimated by the MP2 calculations. However, the calculated *muon* HFCCs using *equilibrium* geometries (entries marked with "H" in Table 1) fall some 10−40 MHz (ca. 5−20%) below the experimental data for the *sec*-butyl radicals in paper II, and also for the Mu−*tert*-butyl data published earlier for muoniated *tert*-butyl in ref 41, for both the MP2 and B3LYP calculations. This difference stems from vibrational effects. As already commented, atoms in molecules are not at rest even at 0 K and zero-point motion then affects the (averaged) HFCCs observed, a dynamical effect that is especially important in the case of Mu-substituted molecules.[8,48−51,53] The light muon mass, about one-ninth that of a proton, makes the average C−Mu bond considerably longer than the C−H bond at the same position in an isotopomer. This vibrational effect cannot be accounted for by the optimized equilibrium geometry, and overlooking it can dramatically underestimate the muon HFCCs, as noted above. Of course, there is a similar vibrational effect on the C−H bond length, but the proton HFCCs are much less affected.[53] We have therefore calculated the *proton* HFCCs on the basis of equilibrium geometries only.

Vibrational Averaging of Muon HFCCs. Conventionally, a molecular vibration is usually decomposed into anharmonic and harmonic components, both of which will affect the averaged properties of molecules. The harmonic correction to HFCCs is believed to be dominant over the anharmonic one for most regular molecules,[32] and this appears to be the case for the low-lying vibrational states of the muoniated ethyl radical as well.[50] For muoniated radicals, vibrational effects become much more dramatic due to increased anharmonicity, especially in the C−Mu stretching mode. Theoretical calculations of HFCCs for small molecular radicals, such as HCO and HOO radicals, showed that the vibrational contributions became much larger when a heavy H atom was replaced by a lighter isotope:[49] up to 45% in the COMu case, though these are α-radicals. Calculations for the muoniated ethyl radical have also shown appreciable anharmonic corrections to the vibrationally averaged β-muon HFCC,[50,51,53,60] and as well for the muoniated methyl radical.[8]

To evaluate vibrational corrections to HFCCs or other molecular properties theoretically, several approaches have been developed. As previously noted, some first-principles attempts to solve the vibrational Schrödinger equation were made by Barone and co-workers by applying perturbation theory within their locally modified code.[52] Instead of a direct analytical analysis, a path-integral Monte Carlo (PIMC) study has also been carried out to calculate averaged HFCCs of the muoniated ethyl radical,[53] and the results of these calculations are compared with our calculations for the Mu−ethyl radical in Table 2. The theoretical results from this PIMC study are also very important for us to benchmark the performance of a third approach to estimate vibrationally corrected HFCCs; namely, by changing geometric properties, and in particular bond lengths, from the optimized equilibrium geometry. This third method is based on a mathematical treatment that proves the anharmonic and partial harmonic corrections to molecular properties can be obtained at the vibrationally averaged geometry.[61]

Exploiting this third approach, and specifically the results of the PIMC study of ref 53, we sought the vibrationally averaged structure of a muoniated radical to calculate anharmonically corrected HFCCs, beginning with the Mu−ethyl radical, which served as a "benchmark" for the methodology, to calculate the HFCCs of the muoniated butyl radicals of interest (Table 1). As expected, the effect of this vibrational averaging is dramatic for the stretching mode of the C−Mu bond, with a thermal-equilibrium bond length at 25 K elongated by a factor of 1.076 in ref 53 compared to its equilibrium value. There is some decrease with temperature in this bond scaling effect, by about 10% up to 300 K, but with a much smaller difference at low temperatures, so this same scale factor of 1.076 has been assumed in the present calculations at 0 K. Though a scale factor of 1.02 is also found due to vibrationally averaged anharmonic corrections in the C−H bond, the effect of this on calculated proton HFCCs is small enough to be ignored, judging from the results of Claxton et al.[51] As previously noted then, the proton HFCCs have been calculated *only* at the equilibrium geometries found in the present study.

Table 3. Scale Factor and Basis Set Variations for the Muon and Proton HFCCs of the Ethyl Radical

β H (eclipsed)	β H (staggered)	β H (averaged)	α H	factor	method
141.4	31.8	68.3	−67.2	1.00	MP2/EPR-III
150.9	31.2	71.1	−66.8	1.05	MP2/EPR-III
156.1	30.6	72.4	−66.5	1.076	MP2/EPR-III
161.6	30.2	74.0	−66.3	1.10	MP2/EPR-III
162.7	40.2	81.1	−62.9	1.00	B3LYP/EPR-III
176.0	38.3	84.2	−58.5	1.05	B3LYP/EPR-III
184.7	37.9	86.8	−58.3	1.076	B3LYP/EPR-III
193.6	37.4	89.5	−58.0	1.10	B3LYP/EPR-III
135.3	30.3	65.3	−72.6	1.00	MP2/EPR-II
150.4	29.2	69.6	−71.8	1.076	MP2/EPR-II
155.4	38.2	77.3	−64.3	1.00	B3LYP/EPR-II
176.8	35.9	82.9	−59.7	1.076	B3LYP/EPR-II
		76(1)	−63(1)	ethyl experimental[13,63] (errors in parentheses)	
151(2)	36(2)	80(2)	−62(1)	Mu−ethyl experimental[13,63] (errors in parentheses)	

Similar C−Mu bond scale factors have been reported by Webster et al.[50] and by Claxton et al.[51,60] for muoniated ethyl, over a range from about 1.05 to 1.10, depending on how one assesses this effect. However, these calculations have adopted a vibrational-perturbative approach with only three active modes to evaluate the effects of bond anharmonicity, in contrast to the more fully quantum multimode analysis of Böhm et al.[53]

It should be noted that the averaged bond distance is not identical to the bond length at the vibrationally averaged geometry but differs by a small amount related to the harmonic vibrational constant.[61,62] In this sense, simply elongating the C−Mu bond by the factor of 1.076 justified above (and in Table 3) can only be regarded as an approximation to the true effective geometry of the muoniated radical. Typical deviations due to harmonic vibrations are reported to be about 10% of the overall HFCC,[32] similar to the deviations found here between theory and experiment near 0 K.

Benchmark Calculations for HFCCs. A study of the hydrogen and muon HFCCs of the unsubstituted and muoniated ethyl radicals was carried out to "benchmark" the performance of the MP2/EPR-III and B3LYP/EPR-III methods applied in the current study, utilizing the bond-elongation scheme of 1.076 for the C−Mu bond proposed above. Comparisons with both experiment and other theoretical methods are given for the eclipsed and staggered conformers for both the unsubstituted and muoniated ethyl radicals in Table 2. The calculated β-proton HFCCs for both are also shown as the averaged values for a "freely-rotating" CH_3 group, $\langle A_\beta \rangle$, which can be directly compared with the experimental EPR data (temperature-independent down to 4 K; see Figure 13 in ref 13), and defined by $\langle A_\beta \rangle = 1/3(A'_\mu + 2A_p)$ for the β-HFCC of $-CH_2Mu$ for the muoniated radical.[13,41]

From Table 2, it is evident that, at the electronic structure level, for the unsubstituted ethyl radical, the MP2 calculation outperforms the B3LYP calculation for β-proton HFCCs in comparison with results from higher-level theories, both at 0 K and for the averaged β-methyl proton HFCCs, $\langle A_\beta \rangle$, as can be seen most completely in comparison with the results from ref 20. In comparison with the experiment for $\langle A_\beta \rangle$ of the unsubstituted ethyl radical, both the MP2 and B3LYP calculated results are about equal, falling below and above experiment by ∼10%, respectively, though somewhat better agreement is found from the B3LYP calculations. The experimental α-proton HFCC (−63 ± 1 MHz) is also well predicted by the B3LYP calculation, better than by MP2. It is noted also that the MP4/EPR-III results for the ethyl radical are very similar to those from the MP2/EPR-III calculations.

For the muoniated ethyl radical, the agreement between theory and experiment for the eclipsed β-muon HFCC at 0 K (151 ± 2 MHz, extrapolated) is also impressive at the MP2/EPR-III level of theory, utilizing the aforementioned scale factor 1.076 for the C−Mu bond. It is important to point out that there is no evidence that the HFCC of the Mu−ethyl radical, $A'_\mu(T)$, is being affected by the phase transition at the melting point of ethylene.[13,50,63] This "phase-free" effect means that the muoniated ethyl radical is a good benchmark system to assess electronic and vibrational effects free from the environmental influence of the surrounding matrix of ethylene molecules. In contrast to the eclipsed bond, the extrapolated staggered proton HFCC to 0 K of $-CH_2Mu$ for muoniated ethyl (36 ± 2 MHz) is better predicted by B3LYP/EPR-III, whereas for the averaged β-methyl HFCC (80 ± 2 MHz) and for the α-proton (−62 ± 1 MHz) HFCC of Mu−ethyl, both the MP2 and B3LYP calculations give much the same level of agreement with the data.

In summary, these benchmark calculations comparing theory and experiment for the ethyl radical clearly favor the MP2/EPR-III calculations for the *muon* HFCC, using the bond-elongation scheme adopted from ref 53, but on balance, favor the B3LYP/EPR-III calculations for the *proton* HFCC, the latter for both the substituted and unsubstituted radical.

Nevertheless, as previously noted, in this study, the results for both the B3LYP and MP2 calculations are presented to provide a more complete picture of the comparison between theory and experiment for the HFCCs of the butyl radicals of interest. In fact, in some cases, the MP2 results are actually in better agreement with experiment for proton HFCCs than the B3LYP

calculations. However, from the comparisons presented in paper II, the excellent agreement often seen from the B3LYP calculations for the muon HFCCs in the solid phase (including at temperatures near 0 K) suggest that these calculations may fortuitously mimic the environmental effect of guest−host interactions in the solid phase, which is addressed further in the discussion that follows.

Though the scaling factor of 1.076 introduced above for the muon HFCCs, along with the use of EPR-III basis sets for both the MP2 and B3LYP calculations, gives good agreement with experiment from the entries in Table 1 for the butyl radicals discussed in paper II, typically at the 10% level or better, and seen as well in the benchmark comparisons shown in Table 2, it is nevertheless of interest to explore just how sensitive the calculated results for HFCCs are to small variations in these scaling factors as well as to explore the effect of a change in basis set, to be able to assess the level of agreement that could inherently be expected between the calculated and experimental values for HFCCs. These comparisons are shown in Table 3 as a further benchmark for the ethyl radical.

First, the top entries for different scale factors for the Mu−ethyl radical exhibit variations of about 2.5% in the eclipsed (muon) HFCC for the MP2/EPR-III calculation, though less for the staggered proton HFCCs, both scaling essentially linearly in this small range. Variations at this level are well within systematic error in determining the experimental values from extrapolation to 0 K. Setting the scale factor to 1.0 gives the same result as for the unsubstituted radical, demonstrating a significant 10% increase in muon HFCC due to vibrational corrections. A larger effect by about a factor of 2 is seen in the case of the B3LYP/EPR-III calculation, which provides another argument in favor of the MP2/EPR-III results for muon HFCC in the absence of lattice interaction effects. Though a case could be made that a smaller scale factor of 1.05 (for MP2/EPR-III) would be in better agreement with the experimental result for $A'_\mu(0) = 151 \pm 2$ MHz, consistent with calculated results reported for Mu−ethyl in ref 50 or refs 51 and 60, it is important to remember here that these smaller scale factors around 1.05 were determined phenomonologically, in contrast to the factor of 1.076 we have utilized, found from the quantum Monte Carlo calculations of ref 53.

Though it is a common view that calculations carried out with larger basis sets (e.g., EPR-III) give superior results to smaller ones (e.g., EPR-II), this could depend on the molecular properties in question, and in particular here, spin densities and HFCCs. To assess this level of sensitivity, we also compare results for calculation of HFCCs with the EPR-II basis set for the ethyl radicals in Table 3 (bottom half). Similar variations are seen as found for the scale factors discussed above, with the EPR-II results even in slightly better agreement with the experimental measurements. Nonetheless, the few megahertz difference is not inconsistent with the expected experimental error. Moreover, in this case, the EPR-III calculations for the *un*substituted ethyl radical (scale factor =1.0) agree better with the MP2 calculations for the staggered protons and with the B3LYP calculations for α-H (cf. Table 2), again though with differences only at the few percent level. Similar differences in HFCCs for the variations shown in Table 3 are observed for the *tert*-butyl radical, but in this case the lattice interaction effects referred to above render the comparison with the experimental value for $A'_\mu(0)$ less meaningful. In fact, even if environmental effects are much less than those seen for muoniated *tert*-butyl (paper II), molecular interactions and vibrational/dynamical effects will always be present at some level and as such are bound to affect the measured HFCCs, rendering the seemingly better agreement noted above for the smaller EPR-II basis set somewhat suspicious, because this comparison impacts only differences in the electronic contributions to HFCCs.

Suffice it to say that we can expect the present calculations for both muon and proton HFCCs for the butyl radicals of interest in paper II, with our assumed muon scale factor of 1.076 and the EPR-III basis set, to be accurate to the 5−10% level, well within "state of the art" and also in accord with experimental error for the results reported in paper II.

RESULTS AND DISCUSSION: COMPARISONS WITH EXPERIMENT

The central outcome of the present work is the calculated muon and proton HFCCs for the butyl radicals given in Table 1. Entries shown are all given in vacuo at 0 K and can be compared with the extrapolated data to 0 K from μSR measurements for muoniated butyl radicals and with the averaged values from early EPR measurements. As previously noted, though not calculated herein, the torsional barriers to internal rotation, determined from model fits to measured temperature-dependent HFCCs reported in paper II, are nevertheless of interest and are discussed on a qualitative basis in support of the results from theory reported in Table 1. Comparisons between theory and experiment are discussed on a case-by-case basis below.

Isobutyl and *tert*-Butyl Radicals Formed from Isobutene. Two muoniated radicals can be formed from muonium addition to isobutene, the Mu−*tert*-butyl (muoniated *tert*-butyl), from Mu addition to the terminal C atom (Figure 2a) and Mu−isobutyl (muoniated isobutyl), from Mu addition to the nonterminal C atom of isobutene (Figure 2b). Our calculations at the MP2/EPR-III level indicate that the isobutyl radical (i1) is 20.6 kJ/mol less stable thermodynamically than the *tert*-butyl radical, suggesting a much weaker experimental signal than for the dominant Mu−*tert*-butyl radical expected to form. Since not reported on in paper II, the isobutyl radical is not discussed further here.

Data for the HFCCs of the Mu−*tert*-butyl radical have been reported earlier by Percival et al. in both the solid and liquid phases,[41] and these results, along with some additional data points taken from the present study at temperatures below 50 K, are given in paper II. The $A'_\mu(T)$ data exhibit a clear "McConnell plateau" at low temperatures, with an extrapolated result to 0 K of 155 MHz that is seemingly in excellent agreement at first glance with the present B3LYP calculations, giving 153.7 MHz for A'_μ at 0 K (Table 1).

However, the benchmark comparisons made with the ethyl radical in Table 2 and the earlier discussion suggest that this seemingly excellent level of agreement is likely fortuitous, due to environmental effects resulting from host−guest (isobutene−*tert*-butyl) interactions that enhance the muon HFCCs in the solid phase and which just happen to be well reproduced by the B3LYP calculations. The MP2 calculations of muon HFCCs are expected to be more reliable in the *absence* of lattice interactions. Experimental evidence for these interactions in the *tert*-butyl case is clearly indicated by the discontinuity or "gap" seen in $A'_\mu(T)$ in ref 41 (reported also in Figure 7 of paper II), where the muon HFCC drops sharply in the liquid phase precisely at the temperature of the solid−liquid phase transition of the isobutene matrix. Similar effects are observed for the *sec*-butyl radicals

formed from 2-butene at the distinct melting points of *cis*- and *trans*-2-butene and are addressed below.

The origin of this gap is unclear. As noted by Percival et al.,[41] the slope of the trend in $A'_\mu(T)$ for Mu−*tert*-butyl changes as a result of the phase change upon the melting of the matrix of host isobutene molecules, suggesting that the origin of the discontinuity seen in $A'_\mu(T)$ at the melting point may be rooted in differences in torsional barriers about the $C_\alpha-C_\beta$ bond for the Mu−*tert*-butyl in the different phases. Internal rotation barriers were determined by fits to the experimental data in ref 41, giving ∼3.4 kJ/mol in the solid phase with a lower barrier of ∼2.3 kJ/mol in the liquid phase, with similar torsional barriers found from the model calculations reported in paper II. These fitted barriers were predicated on the assumption that the muon HFCCs at 0 K in the solid and liquid phases are the same, which is equivalent to the assumption that there is *no* environmental effect on spin-polarization or geometric alteration affecting $A'_\mu(T)$. The higher barrier found in the solid phase is then the result of more hindered internal rotation, which then simply "relaxes" at the phase transition.

An alternate possibility is that environmental effects *do* affect the electron spin density at the muon, and hence the muon HFCC *is* different in the two phases due to differences in polarized spin density or to an altered molecular geometry. It becomes interesting to appreciate then what would happen if we were able to "switch off" the environmental effect due to host−guest interactions. We would then expect the $A'_\mu(T)$ data for Mu−*tert*-butyl in the solid to be shifted well below its extrapolated value to 0 K, where it is actually seen by experiment. Concomitantly, it would also be shifted below the calculated value at 0 K from the B3LYP calculations that agree with the trend in the data, in accord with the benchmark comparisons of Mu−ethyl discussed earlier (Table 2) showing that the B3LYP calculations overestimate the muon HFCC near 0 K. Thus, being consistent as well with these benchmark results, the MP2/EPR-III calculated muon HFCC of 131.1 MHz at 0 K (Table 1) does indeed fall well below both the experimental intercept and the B3LYP-calculated value at 0 K and can also give an equally good fit to the data in the liquid phase (see paper II) as that reported by Percival et al.[41] These effects of distinct changes in torsional barriers that are reflected in the different slopes seen in the liquid and solid phases, and in intrinsic HFCCs at 0 K due to environmental effects, are likely acting synergistically, but with different weightings depending on the nature of the butyl radical that is formed.

***sec*-Butyl Radicals Formed from 2-Butene.** In contrast to the *tert*-butyl case above and *sec*-butyl from 1-butene discussed below, where Mu addition places the muon in a terminal CH_2Mu group, Mu addition to *cis*- or *trans*-2-butene places it at the central methylene position in the *sec*-butyl radical, $CH_3-CHMu-\dot{C}H-CH_3$. In this case, there is only one muoniated structure possible for each 2-butene isomer, in contrast to Mu addition to both isobutene and 1-butene, where different isomeric products can be formed. Experimentally, as seen in Figure 6 of paper II, the two muoniated *sec*-butyl radicals show a clear distinction in $A'_\mu(T)$ for the *sec*-butyls formed from *trans*- and *cis*-2-butene in the solid phase, suggesting preservation of the parent cis and trans geometries. The muon HFCCs from CHMu also demonstrate a rather remarkable sensitivity to these different butene environments, with marked discontinuities seen in $A'_\mu(T)$ at the specific melting points of *cis*- (134 K) and *trans*-2-butene (168 K), behavior that is similar to that seen for the muoniated *tert*-butyl radical. Above ca. 150 K, the muon HFCC of the *sec*-butyl radicals formed from *cis*- and *trans*-2-butene precursors merge into a single curve, demonstrating that the barriers separating local minima on the PES have been mostly overcome, with the different conformations then easily interconvertible.

As in the Mu−*tert*-butyl case previously discussed, the B3LYP calculations in Table 1 for the s1 (trans) isomer (Figure 2d) provide almost quantitative agreement with the trend in the data for the *trans*-2-butyl radical in the solid phase, again mimicking the environmental effect of lattice interactions that are believed to enhance the muon HFCC. The B3LYP-calculated value of 145.2 MHz at 0 K is only a few megahertz above the extrapolated experimental result in paper II, as is the model fit to $A'_\mu(T)$ discussed therein utilizing these B3LYP-calculated muon HFCCs, giving a torsional barrier of 3.0 kJ/mol, essentially the same barrier as found[41] for the *tert*-butyl radical. For the cis isomer (s3, Figure 2f), formed from the separate *cis*-2-butene precusor, the experimental muon HFCC lies a few megahertz above $A'_\mu(T)$ for the trans radical at low temperatures and also has a somewhat steeper falloff, suggesting a lower internal rotation barrier about the $C_\alpha-C_\beta$ bond. This is consistent with theoretical predictions that the cis conformation is associated with a lower backbone torsional barrier than the trans one.[64] However, no energy minimum could be found for the cis isomer from the B3LYP calculation.

In like manner as well to the results for Mu−*tert*-butyl above, the muon HFCC calculated at the MP2 level of theory (126.2 MHz at 0 K, Table 1), falls well below the experimental intercept for *trans*-2-butyl in the solid phase but agrees very well with the fit to the $A'_\mu(T)$ data in the liquid phase reported in paper II. This is consistent with the suggestion advanced earlier that the muon HFCC $A'_\mu(T)$ appear to be intrinsically phase-dependent, such that the MP2 calculations are inherently more accurate in the absence of lattice interactions. This claim is further substantiated by the comparisons between the MP2 theory and experiment for the *sec*-butyl radical formed from 1-butene, discussed below.

With regard to the dramatic gaps seen in $A'_\mu(T)$ for the *tert*-butyl and both *sec*-butyl radicals reported in paper II, precisely at their respective parent alkene melting points, it is noted that these radicals are formed from planar alkenes (isobutene and the *cis*- and *trans*-2-butenes), which can be expected to exhibit different and more ordered packing arrangements in the solid phase compared to the liquid phase. In contrast, 1-butene (discussed below) is dominated by the nonplanar gauche form with a flexible carbon skeleton, suggesting a more disordered environment and which in fact shows no gap in $A'_\mu(T)$ at the bulk melting point.

The muoniated *sec*-butyl radicals formed from *cis*- or *trans*-2-butene have two distinct β-proton environments, the three equivalent protons of the terminal methyl group, and the single proton of the central Mu-substituted methylene group, −CHMu. The *eclipsed* proton of the CH_3 group in *trans*-2-butyl also exhibits a large proton HFCC near 0 K, giving an experimental intercept of ca. 125 MHz, in excellent agreement with theory, but here, anomalously, with the MP2-calculated proton HFCC of 124.1 MHz (atom 10, third entry for s1 in Table 1). Thus, in this case, the B3LYP-calculated result of 134.6 MHz at 0 K is about 10 MHz above the MP2 result and correspondingly gives a poorer account of the trend in the data. The slope of $A_{CH_3}(T)$ for the temperature dependence of the HFCC for the methyl protons of *trans*-2-butyl is very shallow in the solid phase and correspondingly yields a rather high torsional barrier of V_2 = 4.7 kJ/mol from fits to the experimental data in paper II.

This relatively high barrier found is perhaps the result of two synergistic effects: the coupling of this internal rotation about the $C_\alpha-CH_3$ bond to the torsional mode of the carbon skeleton and the presence of muonium in the middle of the backbone chain, in the $CHMu-CH_3$ group. The net effect is that internal rotation about the $CMuH-CH_3$ bond is coupled with the torsion about the $C_\alpha-CMuH$ bond, causing hindered rotation of the terminal β-methyl group,[60] thereby raising the overall internal rotation barrier about the $C_\alpha-CH_3$ bond. This feature may also be responsible for the rather dramatic discontinuity seen for $A_{CH_3}(T)$ at the bulk melting point of *trans*-2-butene (168 K) in Figure 6 of paper II.

Good agreement is seen in paper II between the B3LYP theory and experiment for the *staggered* proton HFCC of the Mu-substituted group, $-CHMu$, both for the calculated trend in $A_{CHMu}(T)$ and for the extrapolated 0 K intercept, with a B3LYP-calculated value of 64.1 MHz, again for the s1 conformer of the *sec*-butyl radical (atom 12, fourth entry for s1 in Table 1). It is noteworthy that the trend seen for $A_{CHMu}(T)$ in Figure 6 of paper II is opposite to that for $A'_\mu(T)$, as expected, and noteworthy as well that only a single proton is involved in the calculation here. The level of agreement seen is also in accord with the benchmark calculations carried out earlier for the staggered protons of $-CH_2Mu$ of the muoniated ethyl radical (Table 2), consistent with the fact that the MP2-calculated result at 0 K is 45.4 MHz for *trans*-2-butene here, much too low to account for the data. This brings back into focus the aforementioned and seemingly anomalous result that much better agreement between theory and experiment was found with the MP2 calculations for the eclipsed methyl proton HFCCs, $A_{CH_3}(T)$, though it is again remarked that these are for eclipsed not staggered protons. That result for $A_{CH_3}(T)$ is believed due to the synergistic couplings noted above, facilitated by the location of the C−Mu bond in the central methylene position, which gives rise to the relatively high torsional barrier of 4.7 kJ/mol seen. This synergism appears to be reflected as well in the barrier to internal rotation found for $A_{CHMu}(T)$ of 5.6 kJ/mol in paper II, utilizing the B3LYP-calculated HFCCs from Table 1.

***sec*-Butyl Radicals Formed from 1-Butene.** Similar to Mu addition to isobutene, which could form both the *tert*-butyl (major product) and isobutyl (minor product) radicals, two distinct isomers can also be formed from Mu/H addition to 1-butene, the dominant *sec*-butyl radical and the minor, primary, *n*-butyl (or 1-butyl) radical, from Mu addition to the central carbon, $CH_3CH_2CHMu\dot{C}H_2$ (n1−n5 in Figure 2). It is also worth recalling that in both the Mu−*tert*-butyl and Mu−*sec*-butyl radicals here, the muon is placed in the terminal methyl group, $-CH_2Mu$, in contrast to the *trans*-2-butyl radical discussed above, where the muon is placed in the central methylene group.

Among the several possible muoniated *sec*-butyl isomers that could be formed from 1-butene, the trans-like *sec*-butyl radical (s1 in Figure 2d) is the most likely candidate for several reasons. First, Mu is favored to add to the gauche form of 1-butene (Figure 3a), which is the least bulky direction, directly yielding the *trans-sec*-butyl (s1) radical, the same radical as formed from *trans*-2-butene discussed above. Second, this adduct is also the most stable isomer among all eight possible radical products from 1-butene (s1, s2, s3, and n1−n5 in Figure 2). Third, supporting evidence provided by the data in Figure 3 of paper II exhibits a large proton HFCC close to 125 MHz near 0 K that can only arise from an eclipsed C−H bond, thus convincingly eliminating the s2 *sec*-butyl radical that has no such bond. Though formation of the cis (s3) isomer remains a possibility, as discussed in paper II, both the muon and proton HFCC do not agree as well with fits to the data as those from the s1 conformer do. Some interconversion between these different conformers could again be expected though at the higher temperatures.

However, unlike the cases of muoniated *tert*-butyl or *sec*-butyl formed from 2-butene discussed above, there is *no obvious* gap seen experimentally in the muon HFCCs $A'_\mu(T)$ at the melting point of 1-butene (88 K). Even though a small gap cannot be completely ruled out, this would still suggest a highly reduced level of lattice interactions in comparison with both the muoniated *tert*-butyl and *sec*-butyl radicals discussed above, perhaps due to the more disordered or polycrystalline nature of 1-butene noted earlier. Accordingly, the muon HFCCs for the muoniated *sec*-butyl radical formed directly from 1-butene are much better accounted for by the MP2-calculated HFCC here, both for the eclipsed C−Mu bond at 0 K, where the theory value of 139.6 MHz (atom 10, fifth entry for s1 in Table 1) falls only about 4 MHz below experiment, and in the fit to $A'_\mu(T)$ from the MP2 calculations here in the model fits of paper II. The torsional barrier determined from this fit is 2.9 kJ/mol, very similar to that found for the muoniated *tert*-butyl radical in ref 41 and in paper II. In contrast, the B3LYP-calculated muon HFCC of 157.2 MHz at 0 K (Table 1) is well above the (extrapolated) experimental result of about 144 MHz, a similar outcome to that seen in benchmark comparisons with the muoniated ethyl radical (Table 2). This result for the muon HFCC of *trans-sec*-butyl from 1-butene provides further evidence supporting the view consistently expressed herein that the MP2 calculation intrinsically gives a better account of the muon HFCC in the *absence* of interactions in the solid state.

This view has its genesis in the aforementioned benchmark calculations for the ethyl radical (Table 2) where the MP2 calculations also gave the best agreement with experiment for the muon HFCCs. It is noteworthy here that ethylene, though planar, in contrast to 1-butene, has reduced polarizability compared to 1-butene, so we may expect both of them to exhibit relatively less variation in different condensed phases compared to isobutene and 2-butene. Thus, it is fair to speculate that the muoniated adducts formed from 1-butene and ethylene will be much less influenced by the phase transition at their respective precursor melting points, and their radical products indeed do not exhibit any obvious gap in $A'_\mu(T)$ at such temperatures.

The most stable *n*-butyl radical is the n3 conformer (Figure 2i), expected to be favorably formed from the more stable gauche form of its 1-butene precursor, and which is also facilitated as the product of Mu/H addition to gauche 1-butene from a less hindered direction. However, like the isobutyl radical from isobutene, it is expected to have minor presence and has only been tentatively identified in paper II, so is also not discussed further.

As in the case of the methyl protons of *trans*-2-butyl above, there is also a large proton HFCC for the *sec*-butyl from 1-butene at 0 K in Figure 3 of paper II, due to an eclipsed proton of the unsubstituted β-methylene group, $-CH_2$. The B3LYP-calculated value of 124.2 MHz for the trans s1 conformer (atom 11, sixth entry for s1 in Table 1) is in good agreement with the extrapolated experimental intercept, and consistent as well with the fit to the temperature-dependence of the experimental HFCC for $A_{CH_2}(T)$ in the solid phase. These proton HFCC data also exhibit a discontinuity at the melting point of 1-butene, though the gap is not nearly so dramatic as for the *trans*-2-butyl data in Figure 6 of paper II. While a good fit to the data for

$A_{CH_2}(T)$ is obtained from the B3LYP-calculated HFCC in the solid, it was not possible to simultaneously fit the data in the solid and liquid phases with these calculated HFCCs, the latter being much better accounted for by the MP2-calculated HFCC, with a 0 K intercept of 113.4 MHz for the s1 conformer (atom 11, fifth entry in Table 1), well below that for the B3LYP calculations.

This situation is reminiscent of that for the muon and proton HFCCs of the *trans*-2-butyl radical discussed above, both data sets suggesting that environmental effects also impact on *proton* HFCCs. However, in contrast to *trans*-2-butyl, the fitted torsional barriers in paper II are quite low, 1.4 kJ/mol in the solid and 1.5 kJ/mol in the liquid. An important difference between the *sec*-butyl radicals formed from 2-butene and, here, 1-butene, is that the Mu atom adds to the terminal carbon in 1-butene but to a central carbon in 2-butene. Hence the synergistic effect discussed above between the internal rotation of the C−Mu bond and the backbone distortion of the carbon chain in the case of *trans*-2-butyl is largely missing in the present case, likely explaining the much reduced barriers seen for the methylene protons here. This probably also lies at the heart of why it is the MP2 calculations that give better fits for the methyl proton HFCCs, $A_{CH_3}(T)$, for *trans*-2-butyl in the solid phase, in contrast to the better result found here from the B3LYP calculations for $A_{CH_2}(T)$. It is also possible that fast interconversion between energetically close-lying conformers is contributing to the relatively low barriers found here.

The HFCCs of the staggered protons of the terminal CH_2Mu group were also observed in the *sec*-butyl data from 1-butene in Figure 3 of paper II and again are in excellent agreement with the B3LYP calculations, both near 0 K and in the overall fitted trend with temperature, $A_{CH_2Mu}(T)$. In this case, as for $A_{CHMu}(T)$ for *trans*-2-butyl (Figure 6 in paper II), there is no discontinuity at the phase transition, and the good agreement found in fitted trends with temperature for B3LYP-calculated staggered proton HFCCs is again consistent with the benchmark calculations discussed above for the ethyl radical (Table 2).

■ CONCLUDING REMARKS

The HFCCs of muoniated butyl isomers, formed from muonium addition to the parent butenes, have been investigated by ab initio theory using the Guassian03 suite of programs. On the basis of comparisons with experiment (paper II) near 0 K, the muon adducts are confirmed to be Mu-eclipsed radicals. The equilibrium geometries of the butene precursors and Mu-radical products were established by using both B3LYP/EPR-III and MP2/EPR-III calculations, with MP2 found to be more reliable in predicting stable conformers. All calculations were carried out in vacuo at 0 K assuming the validity of the BO approximation.

A self-consistent first-principles calculation of vibrational contributions to these HFCCs has not been attempted but rather we have tried to account for such effects by a C−Mu bond elongation scheme in which a scaling factor of 1.076, determined from the quantum Monte Carlo calculations of Böhm et al. for the Mu−ethyl radical,[53] was introduced to alter the equilibrium geometry, with the muon HFCC calculations then carried out on this modified albeit static structure. Comparisons with different scale factors that have been varied by a few percent as well as comparisons of the results of EPR-II and EPR-III basis sets that have also been carried out demonstrate that the calculated results for both muon and proton HFCCs for the butyl radicals of interest reported herein can be expected to be reliable to the 5−10% level.

Comparisons of these calculated HFCCs with experiment are complicated by phase transitions between solid and liquid in both cases of the muoniated *tert*-butyl and *sec*-butyl radicals, formed from planar isobutene and 2-butene isomers, respectively, where the experimental temperature dependences of the muon HFCCs, $A'_\mu(T)$, exhibit marked discontinuities at the melting points of the alkene precursors. These discontinuities signify a large contribution to muon HFCCs from environmental effects due to lattice interactions in the solid phase, where the experimental values appear to be best predicted by the B3LYP/EPR-III calculations. In contrast, the MP2/EPR-III calculations yield better agreement between theory and experiment for the muon HFCC of these butyl radicals in the liquid phase, predicting HFCC at 0 K well below the B3LYP results.

The experimental result for the muon HFCC at 0 K for the *sec*-butyl radical formed from 1-butene (paper II) is markedly different compared to the result for both the muoniated *tert*-butyl and *trans*-2-butyl radicals. In contrast to those cases, the *sec*-butyl formed from 1-butene exhibits no obvious gap in $A'_\mu(T)$ at the bulk melting point, indicating that environmental effects on the muon HFCC are relatively unimportant in this case. This may be a consequence of the fact that the carbon skeleton of the 1-butene precursor is nonplanar, in contrast to that of isobutene and 2-butene. As a result, much better agreement between theory and experiment for $A'_\mu(T)$ is found across the phase transition from the MP2 calculations in accord with expectations from "benchmark" calculations carried out for the muoniated ethyl radical, which also exhibits no discontinuity in $A'_\mu(T)$ at the bulk melting point, and where better agreement with experiment is also found near 0 K. In both of these cases, the B3LYP-calculated result is well above the experimental data.

The MP2/EPR-III calculations appear to give the best intrinsic agreement with higher level calculations as well as experimental muon HFCCs in the *absence* of appreciable host−guest interactions. This suggests that the seemingly good agreement found with experiment for the *tert*-butyl and *trans*-2-butyl radicals from the B3LYP/EPR-III calculations below the melting point is likely fortuitous, due to error cancellations in the method, causing these DFT-calculated results to effectively mimic the effect of host−guest interactions in the solid phase.

Since the marked discontinuities seen in muon HFCCs at melting points is only observed for the planar alkene parents (isobutene and 2-butenes), it suggests that more ordered environments facilitate enhanced muon HFCCs in the solid phase, in contrast to the less ordered or more polycrystalline environment of 1-butene, where the *sec*-butyl formed exhibits no such clear discontinuity in $A'_\mu(T)$. However, establishing the reason(s) for this phenomenon from first-principles calculations would involve including the environment effects of radical-host interactions on the muon HFCCs, which is well beyond the level of the calculations reported here.

In contrast to the muon HFCCs, the β-proton HFCCs are, by and large, better predicted by the B3LYP/EPR-III calculations in both phases, though here too there are caveats that need to be made. Large proton HFCCs near 0 K, due to eclipsed C−H bonds in like manner to C−Mu, are observed in the *sec*-butyl radicals, from the methylene protons, $A_{CH_2}(T)$, in the *sec*-butyl radical from 1-butene, and from the protons of the terminal methyl group, $A_{CH_3}(T)$, in the *trans*-2-butyl radical. In the case of $A_{CH_2}(T)$ from 1-butene, the B3LYP-calculated HFCCs agree

well near 0 K with the extrapolated data from paper II, as do the model fits to the temperature dependence for these proton HFCCs. On the other hand, for $A_{CH_3}(T)$ from *trans*-2-butyl, the best agreement with the data in the solid phase, both near 0 K and its temperature dependence, is found with the MP2-calculated HFCCs, a seemingly anomalous result in view of the generally good level of agreement found from B3LYP calculations of proton HFCCs in all other cases.

Both the proton HFCCs $A_{CH_2}(T)$ from 1-butene and $A_{CH_3}(T)$ from *trans*-2-butene exhibit clear and unprecedented discontinuities in their temperature dependences at bulk melting points in paper II, and most dramatically so for the terminal methyl group in the *trans*-2-butyl radical, demonstrating, for the first time, that lattice-interaction effects also influence proton HFCCs. In the liquid phase, it is the MP2 calculations that give the best agreement with the data for $A_{CH_2}(T)$ from 1-butene but this is also true for $A_{CH_3}(T)$ from *trans*-2-butene in the solid phase, suggested above as being anomalously so. In the latter case in particular, coupling of the internal rotation about both the CMu$-$C$_\alpha$ bond at the central methylene position and about the C$_\alpha-$CH$_3$ bond with the carbon backbone torsion in the *sec*-butyl radical, may enhance the barrier to internal rotation for the methyl protons of the muoniated *trans*-2-butyl radical, thus possibly explaining both the high fitted barrier found in paper II and the better agreement found in proton HFCC from the MP2 calculation.

The *staggered* proton HFCCs of the $-$CH$_2$ protons in the *sec*-butyl radical from 1-butene and of the $-$CHMu proton in the *trans-sec*-butyl radical from 2-butene, both consistently give much better agreement with the B3LYP-calculated HFCCs than with MP2, the clearest case perhaps of matching the predictions of the benchmark calculations carried out herein for the muoniated ethyl radical. In both cases, the temperature dependences mirror those of the corresponding muon HFCCs, $A'_\mu(T)$, as expected, but with lower barrier heights, indicative of non-rigid-rotor internal rotation.

Though mindful of the exceptions noted above, the apparent general level of success found here with the B3LYP/EPR-III method employed in our calculations of proton HFCCs may have its roots in the parametrization of the basis set that evolved during the development of EPR-II and EPR-III basis sets using spin-unrestricted Kohn$-$Sham equations.[33] The parametrization of these basis sets is determined in part from optimizing comparisons with experiment for EPR measurenents of isotropic and anisotropic hyperfine coupling constants, yet conceals and mixes some important underlying physics, such as correlation effects, dynamic/vibrational effects, and environment or lattice interaction effects. Especially for hydrogen, the optimal 1s shell basis function contraction scheme for an isolated H atom HFCC can be quite different from that of hydrogen atoms in molecules. That is, the specialized treatment that emerged from designing the EPR-II/EPR-III basis sets, by fitting to molecular computations, likely particularly benefits the comparison between calculated and *averaged* experimental values of proton HFCCs in unsubstituted molecules. On the other hand, this beneficial effect may be considerably reduced or possibly even act in the opposite direction in the case of isotopically substituted molecules and notably here for muoniated radicals, particularly when calculations of individual 0 K proton/muon HFCCs are performed.

Finally, to echo a previous remark, all the calculations in this paper have been carried out within the limits of the BO approximation. This well-known approximation is usually adequate for many property calculations, including HFCCs of ordinary chemical species whose nuclear masses are overwhelmingly large compared to the electron mass. However, it is certainly less valid for muoniated species where the muon mass is only 206 times the electron mass[1,2,44,53] such that the basic assumption of a single nuclear configuration may begin to break down. Since quantum tunneling is known to be prominent in Mu reactivity, and particularly in its addition reactions to alkene double bonds,[3] there could also be some muonium tunneling effects altering muon positions in the muoniated butyl radicals studied here, which could also impact the simple model for the torsional barrier adopted in paper II.[53] In any muon-containing species, there has to be some concern that the motion of the muon is not as separable from the electron motion as in the case of normal H-atoms in unsubstituted molecules.

■ ASSOCIATED CONTENT

Supporting Information. Effects of Hamiltonians and basis sets on the torsional potential energy surface of the *sec*-butyl radical. This material is available free of charge via the Internet at http://pubs.acs.org.

■ AUTHOR INFORMATION

Corresponding Author
*E-mail: yawang@chem.ubc.ca.

■ ACKNOWLEDGMENT

We gratefully acknowledge the financial support for this project provided by "Discovery Grants" awarded to D.G.F. and Y.A.W. from the Natural Sciences and Engineering Research Council of Canada (NSERC).

■ REFERENCES

(1) Roduner, E. *Chem. Soc. Rev.* **1993**, *22*, 337–346.
(2) Roduner, E. *Appl. Magn. Reson.* **1997**, *13*, 1–14.
(3) Garner, D. M.; Fleming, D. G.; Arseneau, D. J.; Senba, M.; Reid, I. D.; Mikula, J. *J. Chem. Phys.* **1990**, *93*, 1732–1740.
(4) Ghandi, K.; Bridges, M. D.; Arseneau, D. J.; Fleming, D. G. *J. Phys. Chem. A* **2004**, *108*, 11613–11625.
(5) Pan, J. J.; Arseneau, D. J.; Senba, M.; Garner, D. M.; Fleming, D. G. *J. Chem. Phys.* **2006**, *125*, 014307–014319.
(6) Oganesyan, V. S.; Cammidge, A. N.; Hopkins, G. A.; Cotterill, F. M.; Reid, I. D.; Jayasooriya, U. A. *J. Phys. Chem. A* **2004**, *108*, 1860–1866.
(7) Pratt, F. L.; Blundell, S. J.; Jestädt, T.; Lovett, B. W.; Macrae, R. M.; Hayes, W. *Magn. Reson. Chem.* **2000**, *38*, S27–S32.
(8) McKenzie, I.; Brodovitch, J. C.; Ghandi, K.; McCollum, B. M.; Percival, P. W. *J. Phys. Chem. A* **2007**, *111*, 10625–10634.
(9) Macrae, R. M.; Carmichael, I. *Physica B* **2003**, *326*, 81–84.
(10) Percival, P. W.; Brodovitch, J. C.; Ghandi, K.; McCollum, B. M.; McKenzie, I. *J. Am. Chem. Soc.* **2005**, *127*, 13714–13719.
(11) Ghandi, K.; Zahariev, F. E.; Wang, Y. A. *J. Phys. Chem. A* **2005**, *109*, 7242–7250.
(12) Fleming, D. G.; Shelley, M. Y.; Arseneau, D. J.; Senba, M.; Pan, J. J. *J. Phys. Chem. B* **2002**, *106*, 6395–6407.
(13) Bridges, M. D.; Arseneau, D. J.; Fleming, D. G.; Ghandi, K. *J. Phys. Chem. C* **2007**, *111*, 9779–9793.
(14) Fleming, D. G.; Bridges, M. D.; Arseneau, D. J.; Chen, Y. K.; Wang, Y. A. *J. Phys. Chem. A* **2011**, doi:10.1021/jp109676b.
(15) Krusic, P. J.; Jesson, J. P.; Meakin, P. *J. Phys. Chem.* **1971**, *75*, 3438–3453.

(16) Carmichael, I. *J. Phys. Chem.* **1985**, *89*, 4727–4732.
(17) Carmichael, I. *J. Phys. Chem.* **1986**, *90*, 2057–2060.
(18) Overill, R. E. *J. Comput. Chem.* **1991**, *12*, 231–236.
(19) Meyer, W. *J. Chem. Phys.* **1969**, *51*, 5149–5162.
(20) Carmichael, I. *J. Phys. Chem.* **1991**, *95*, 6198–6201.
(21) Fernandez, B.; Jørgensen, P.; Byberg, J.; Olsen, J.; Helgaker, T.; Jensen, H. J. A. *J. Chem. Phys.* **1992**, *97*, 3412–3419.
(22) Perera, S. A.; Salemi, L. M.; Bartlett, R. J. *J. Chem. Phys.* **1997**, *106*, 4061–4066.
(23) Petraco, N. D. K.; Wesolowski, S. S.; Leininger, M. L.; Schaefer, H. F., III. *J. Chem. Phys.* **2000**, *112*, 6245–6254.
(24) Xiao, H. Y.; Liu, Y. J.; Fang, W. H.; Liu, R. Z.; Shiotani, M. *J. Theo. Comput. Chem.* **2008**, *7*, 879–887.
(25) Liu, Y. J.; Huang, M. B. *J. Mol. Struct. (THEOCHEM)* **2001**, *536*, 133–142.
(26) Hermosilla, L.; Calle, P.; de la Vega, J. M. G.; Sieiro, C. *J. Phys. Chem. A* **2005**, *109*, 1114–1124.
(27) Kaupp, M.; Bühl, M.; Malkin, V. G. *Calculation of NMR and EPR Parameters*; Wiley-VCH Verlag: New York, 2004; pp 483−504.
(28) Munzarová, M.; Kaupp, M. *J. Phys. Chem. A* **1999**, *103*, 9966–9983.
(29) Carmichael, I. *J. Phys. Chem. A* **1997**, *101*, 4633–4636.
(30) Carmichael, I. *J. Phys. Chem.* **1991**, *95*, 108–111.
(31) Gauld, J. W.; Eriksson, L. A.; Radom, L. *J. Phys. Chem. A* **1997**, *101*, 1352–1359.
(32) Improta, R.; Barone, V. *Chem. Rev.* **2004**, *104*, 1231–1253.
(33) Barone, V. Structure, Magnetic Properties and Reactivities of Open-Shell Species from Density Functional and Self-Consistent Hybrid Methods. In *Recent Advances in density functional methods*; Chong, D. P., Ed.; World Scientific Publishing Co.: Singapore, 1996; Chapter 8, pp 287−334.
(34) Wong, M. W.; Radom, L. *J. Phys. Chem.* **1995**, *99*, 8582–8588.
(35) Byrd, E. F. C.; Sherrill, C. D.; Head-Gordon, M. *J. Phys. Chem. A* **2001**, *105*, 9736–9747.
(36) King, R. A.; Crawford, T. D.; Stanton, J. F.; Schaefer, H. F., III. *J. Am. Chem. Soc.* **1999**, *121*, 10788–10793.
(37) Karpfen, A.; Choi, C. H.; Kertesz, M. *J. Phys. Chem. A* **1997**, *101*, 7426–7433.
(38) Viruela, P. M.; Viruela, R.; Ortí, E.; Brédas, J. L. *J. Am. Chem. Soc.* **1997**, *119*, 1360–1369.
(39) Sancho-García, J. C.; Karpfen, A. *Theor. Chem. Acc.* **2006**, *115*, 427–433.
(40) Zhao, Y.; Truhlar, D. G. *J. Chem. Theory Comput* **2007**, *3*, 289–300.
(41) Percival, P. W.; Brodovitch, J. C.; Leung, S. K.; Yu, D.; Cox, S. F. J. *Chem. Phys.* **1988**, *127*, 137–147.
(42) Fleming, D. G.; Arseneau, D. J.; Pan, J. J.; Shelley, M. Y.; Senba, M.; Percival, P. W. *Appl. Magn. Reson.* **1997**, *13*, 181–194.
(43) Vujoševíc, D.; Dilger, H.; McKenzie, I.; Martyniak, A.; Scheuermann, R.; Roduner, E. *J. Phys. Chem. B* **2007**, *111*, 199–208.
(44) Mielke, S. L.; Schwenke, D. W.; Peterson, K. A. *J. Chem. Phys.* **2005**, *122*, 224313–224321.
(45) Lee, C.; Yang, W.; Parr, R. G. *Phys. Rev. B* **1988**, *37*, 785–789.
(46) Becke, A. D. *J. Chem. Phys.* **1993**, *98*, 5648–5672.
(47) Frisch, M. J. et al. *Gaussian 03*; Gaussian, Inc.: Wallingford, CT, 2004.
(48) Roduner, E.; Reid, I. D. *Isr. J. Chem.* **1989**, *29*, 3–11.
(49) Thomas, S. L.; Carmichael, I. *Physica B* **2006**, *374*−*375*, 290–294.
(50) Webster, B.; Buttar, D. *J. Chem. Soc., Faraday Trans.* **1996**, *92*, 2331–2334.
(51) Claxton, T. A.; Graham, A. M.; Cox, S. F. J.; Maric, D. M.; Meier, P. F.; Vogel, S. *Hyperfine Interact.* **1990**, *65*, 913–926.
(52) Barone, V. *J. Chem. Phys.* **2005**, *122*, 014108–014116.
(53) Böhm, M. C.; Ramirez, R.; Schulte, J. *Mol. Phys.* **2005**, *103*, 2407–2436.
(54) Bell, S.; Drew, B. R.; Guirgis, G. A.; Durig, J. R. *J. Mol. Struct.* **2000**, *553*, 199–219.
(55) Kondo, S.; Hirota, E.; Morino, Y. *J. Mol. Spectrosc.* **1968**, *28*, 471–489.
(56) Durig, J. R.; Compton, D. A. C. *J. Phys. Chem.* **1980**, *84*, 773–781.
(57) Wu, F.; Chen, X.; Shan, X.; Tian, S. X.; Li, Z.; Xu, K. *J. Phys. Chem. A* **2008**, *112*, 4360–4366.
(58) Barone, V.; Adamo, C.; Grand, A.; Brunel, Y.; Fontecave, M.; Subra, R. *J. Am. Chem. Soc.* **1995**, *117*, 1083–1089.
(59) Houk, K. N.; M. N. Paddon-Row, D. C. S.; Rondan, N. G.; Nagase, S. *J. Org. Chem.* **1986**, *51*, 2874–2879.
(60) Claxton, T. A.; Graham, A. M. *J. Chem. Soc., Faraday Trans. 2* **1987**, *83*, 2307–2317.
(61) Lounila, J.; Wasser, R.; Diehl, P. *Mol. Phys.* **1987**, *62*, 19–31.
(62) Morino, Y.; Kuchitsu, K.; Oka, T. *J. Chem. Phys.* **1962**, *36*, 1108–1109.
(63) Yu, D. *Ph.D. thesis*, Department of Chemistry, Simon Fraser University, Canada, 1990.
(64) Chen, Y.; Rauk, A.; Tschuikow-Roux, E. *J. Phys. Chem.* **1990**, *94*, 6250–6254.